NATIONAL ADVISORY COMMITTEE
FOR AERONAUTICS

TECHNICAL NOTE 3323

CHARTS FOR ESTIMATING PERFORMANCE OF

HIGH-PERFORMANCE HELICOPTERS

By Alfred Gessow and Robert J. Tapscott

Langley Aeronautical Laboratory
Langley Field, Va.

NACA

Washington

January 1955

NATIONAL ADVISORY COMMITTEE FOR AERONAUTICS

TECHNICAL NOTE 3323

CHARTS FOR ESTIMATING PERFORMANCE OF

HIGH-PERFORMANCE HELICOPTERS

By Alfred Gessow and Robert J. Tapscott

SUMMARY

Theoretically derived charts showing the profile-drag—thrust ratio are presented for a helicopter rotor operating in forward flight and having hinged rectangular blades with a linear twist of -8°. The charts, showing the profile-drag characteristics of the rotor for various combinations of pitch angle, ratio of thrust coefficient to solidity, and a parameter representing shaft power input, are presented for tip-speed ratios ranging from 0.05 to 0.50. In addition, the ratio of thrust coefficient to solidity as a function of inflow ratio and blade pitch angle is presented in chart form.

The charts of this paper differ from the rotor performance papers previously published by the National Advisory Committee for Aeronautics in that the theory on which the charts are based includes an approximate allowance for stall in the reversed-flow region and contains no small-angle assumptions regarding blade-section inflow angles and velocities. The charts of this paper are therefore considered more accurate than previous ones for flight conditions involving high inflow velocities and large regions of reversed velocity that may be encountered by high-performance helicopters. The assumption is made, however, that outside of the reversed-velocity region, the section angles of attack are small; thus the angles can be replaced by their sine. In addition, other than including an approximate allowance for stall in the reversed-velocity region, the charts do not include stall and compressibility effects.

The charts may be used to study the effects of design changes on rotor performance and to indicate optimum performance conditions, as well as to estimate quickly rotor performance in forward flight. They are also useful in obtaining inflow-ratio and pitch-angle values for use in calculating flapping coefficients and spanwise loadings. The method of applying the charts to performance estimation is illustrated through sample calculation of a typical rotor-performance problem.

INTRODUCTION

Equations were presented in reference 1 from which the thrust, the accelerating and decelerating torque, and the profile-drag power of a hinged rotor operating at high tip-speed ratios and inflow angles could be calculated. Because the equations do not place any limitation on the magnitude of the inflow angle or on the rotor angle of attack, they are considered more accurate than previous analyses when applied to high-speed helicopters and to certain types of convertible aircraft. This paper is an extension of reference 1 in that the equations of that reference are used as the basis of a method for calculating the performance of lifting rotors over a wide range of operating conditions.

Because the basic equations are lengthy, the application of the method is considerably simplified by presenting the more lengthy equations in the form of charts from which rotor performance can be quickly estimated. The charts cover operation at any rotor angle of attack at tip-speed ratios varying from 0.05 to 0.50 for blades that are twisted -8° (blade pitch angles at the tip 8° lower than at the root). With the exception of an approximate allowance for stall in the reversed-velocity region, the charts do not include stall and compressibility effects.

Limit lines showing conditions for which blade angles of attack exceed specified values at given radial stations are included in the charts. These limit lines are useful in determining operating conditions at which stalling begins and for determining the limiting operating conditions.

SYMBOLS

a slope of curve of section lift coefficient against section angle of attack, per radian (assumed equal herein to 5.73)

b number of blades per rotor

C_L rotor lift coefficient, $\dfrac{L}{\frac{1}{2}\rho V^2 \pi R^2}$

C_P rotor-shaft power coefficient, $\dfrac{P}{\pi R^2 \rho (\Omega R)^3}$

C_T rotor thrust coefficient, $\dfrac{T}{\pi R^2 \rho (\Omega R)^2}$

c   blade section chord, ft

c_e equivalent blade chord (weighted on thrust basis), $\dfrac{\displaystyle\int_0^R cr^2 dr}{\displaystyle\int_0^R r^2 dr}$, ft

c_{d_o} section profile-drag coefficient

c_l section lift coefficient

D_p helicopter parasite drag, lb

$(D/L)_o$ rotor profile drag-lift ratio

f   parasite-drag area, $\dfrac{D_p}{\frac{1}{2}\rho V^2}$, sq ft

I_1 mass moment of inertia of blade about flapping hinge, slug-ft^2

L   rotor lift, lb

P   rotor-shaft power, ft-lb/sec

P/L   shaft-power parameter, where P (in this ratio only) is equal to rotor-shaft power divided by velocity along flight path and is therefore also equal to drag force that could be overcome by shaft power at flight velocity

R   blade radius measured from center of rotation, ft

r   radial distance from center of rotation to blade element, ft

T   rotor thrust, lb

V   true airspeed of helicopter along flight path, fps

v   induced velocity at rotor (always positive), fps

W   helicopter gross weight, lb

x   ratio of blade-element radius to rotor-blade radius, r/R

α rotor angle of attack; angle between axis of no feathering (that is, axis about which there is no cyclic-pitch change) and plane perpendicular to flight path, positive when axis is inclined rearward, deg

α_r blade-element angle of attack, measured from line of zero lift, deg (when used in three-term drag polar in fig. 1(b), α_r is expressed in radians)

$\alpha_{(x)(\psi)}$ blade-element angle of attack at any radial position x and at any blade azimuth angle ψ, deg; for example, $\alpha_{(1.0)(270°)}$ is blade-element angle of attack at tip of retreating blade at 270° azimuth position

$\alpha_{(u_T=0.4)(270°)}$ blade-element angle of attack at radius at which tangential velocity equals 0.4 tip speed and at 270° azimuth position, deg

γ flight-path angle (positive in climb, negative in glide), deg

$\theta_{.75}$ blade-section pitch angle at 0.75 radius; angle between line of zero lift of blade section and plane perpendicular to axis of no feathering, deg

θ_1 difference between blade root and blade-tip pitch angles, positive when tip angle is larger, deg

λ inflow ratio, $\dfrac{V \sin \alpha - v}{\Omega R}$

μ tip-speed ratio, $\dfrac{V \cos \alpha}{\Omega R}$

ρ mass density of air, slugs/cu ft

σ rotor solidity, $bc_e/\pi R$

ψ blade azimuth angle measured from downwind position in direction of rotation, deg

Ω rotor angular velocity, radians/sec

Subscripts:

c   climb

i   induced

o   profile

p   parasite

v   vertical component

METHOD OF ANALYSIS

The performance method presented herein utilizes the equations developed in reference 1 for blade-flapping coefficients, rotor thrust, torque, and profile-drag power and also, with some modifications, the energy performance analysis described in reference 2. Inasmuch as the performance method described herein is based on the equations developed in reference 1, the assumptions and limitations incorporated in the reference equations also apply to the performance calculations. (The effects of the primary assumptions and limitations are discussed subsequently in the section entitled "Range of Application of Charts.")

In utilizing the equations of reference 1 to compute rotor performance, numerical substitutions regarding section lift and drag characteristics were made by using the values shown in figure 1. The values of c_l and c_{d_o} below the stall given in the figure are representative of "semismooth" blades and are the same values used in the construction of the charts of reference 2. The values of c_l and c_{d_o} above the stall are based to some extent on wind-tunnel data presented in reference 3, and are presented in figure 1 on the concept of a 360° angle-of-attack range. This concept is useful in the analysis because the angle of attack in the reversed-velocity region can exceed 180°.

By following the procedure of reference 1, it was assumed that the thrust, torque, and power contributions of the reversed-velocity region could be approximated by using constant lift and drag coefficients corresponding to a single representative section angle of attack. For each flight condition, the representative angle was computed at a radial station about one-third of the distance from the center of rotation to the outboard edge of the reversed-velocity region and at an azimuth angle of 270°. The forces at this radial station were found to represent approximately the average of the forces in the reversed-velocity region from plots of the radial distribution of the forces determined from step-by-step calculations for several sample cases. The values of c_l and c_{d_o} corresponding to the representative angle of attack were obtained from figure 1. Although some uncertainty as to the maximum value of c_{d_o} in the 90° angle-of-attack region exists, it was found that the use of a maximum value of 2.0, for example, instead of 1.6 had a negligible effect on the chart values over the range of applicability of the charts.

Fundamental Performance Equation

The power supplied at the rotor shaft of a helicopter is expended in overcoming the rotor profile-drag losses, the induced drag losses, and the parasite-drag losses and in changing the potential energy of the aircraft in climb. The division of shaft power between the various sources can be written in coefficient form as

$$C_P = C_{P_O} + C_{P_i} + C_{P_p} + C_{P_c} \tag{1}$$

In presenting the relationship between C_P and C_{P_O} for various flight conditions in chart form, the resulting plots are greatly clarified if the power-coefficient ratios are divided by the thrust coefficient. Thus,

$$\frac{C_P}{C_T} = \frac{C_{P_O}}{C_T} + \frac{C_{P_i}}{C_T} + \frac{C_{P_p}}{C_T} + \frac{C_{P_c}}{C_T} \tag{2}$$

Each ratio of power coefficient to thrust coefficient in equation (2) may be considered alternately as either an equivalent drag-thrust ratio (wherein the equivalent drag is equal to the drag force that would absorb the power at a velocity equal to ΩR) or as an efficiency factor representing power per unit thrust at a given tip speed.

Almost any problem in helicopter performance, whether it be to determine the shaft power required to maintain a steady-flight condition, the rate of climb at a given power condition, or the top speed of a given helicopter can be solved by means of the fundamental power relation expressed by equation (2). It will be noted that the familiar P/L, $(D/L)_O$, . . . notation used in previous NACA helicopter performance papers is replaced herein by C_P/C_T, C_{P_O}/C_T, ... The power coefficients are based on the relatively constant ΩR instead of on V; thus, the notation used herein avoids having the equivalent drag approach infinity as the forward speed approaches zero. For the same reason, rotor lift L — based on C_L, which is dependent on forward speed — is replaced by the rotor thrust T inasmuch as C_T is independent of forward speed. The conversion of one form of ratio to another is simply:

$$\left.\begin{aligned} \frac{C_P}{C_T} &= \frac{P}{L}\,\mu \\[2ex] \frac{C_{P_O}}{C_T} &= \left(\frac{D}{L}\right)_O \mu \\[2ex] &\quad \bullet \ \ \bullet \ \ \bullet \ \ \bullet \ \ \bullet \end{aligned}\right\} \tag{3}$$

Relations Required in Performance Calculations

Formulas that are necessary for evaluating helicopter performance by means of equation (2) are listed as follows:

$$T \cos(\alpha + \gamma) = W + D_p \sin \gamma \tag{4}$$

$$\frac{C_P}{C_T} = \frac{P}{(\Omega R)T} \tag{5}$$

$$\frac{C_{P_0}}{C_T} = \frac{P_0}{(\Omega R)T} \tag{6}$$

$$\frac{C_{P_i}}{C_T} = \frac{C_T}{2\mu \left[1 + (\lambda/\mu)^2\right]^{1/2}} \tag{7}$$

$$\frac{C_{P_p}}{C_T} = \frac{1}{2C_T} \frac{f}{\pi R^2} \frac{\mu^3}{\cos^3 \alpha} \tag{8}$$

$$\frac{C_{P_c}}{C_T} = \sin \gamma \left[- \sin \gamma \frac{C_{P_p}}{C_T} \frac{\cos \alpha}{\mu} + \sqrt{1 - \cos^2 \gamma \left(\frac{C_{P_p}}{C_T}\right)^2 \frac{\cos^2 \alpha}{\mu^2}} \right] \frac{\mu}{\cos \alpha} \tag{9}$$

$$\tan \alpha = \frac{\lambda}{\mu} + \frac{C_T}{2\mu^2 \left[1 + (\lambda/\mu)^2\right]^{1/2}} \tag{10}$$

These equations, with the exception of equation (9), are similar to those derived in chapter 9 of reference 4 except for the factor $\mu/\cos \alpha$. Equation (9) includes a drag term and is derived from a corresponding equation presented in the appendix of reference 5 by using a multiplying factor of $\mu/\cos \alpha$.

Performance Charts

The calculation of the various C_P/C_T ratios in equations (5) to (9) can be greatly simplified by means of charts that relate the more lengthy ratios to the fundamental variables λ, $\theta_{.75}$, and μ and to each other. Such charts are presented in figures 2 to 4, and their use is demonstrated in succeeding sections of this paper.

Each chart of figure 2 gives $2C_T/\sigma a$ as a function of λ and $\theta_{.75}$ for fixed values of μ ranging from 0.05 to 0.50. In figure 3, C_{P_0}/C_T is shown as a function of C_P/C_T, $2C_T/\sigma a$, and $\theta_{.75}$ for fixed values of μ ranging from 0.05 to 0.50. Also, stall limit lines, the significance of which is discussed in references 2 and 6, are shown in these plots. Figure 4 is a graphical presentation of equation (9) from which the climb

parameter $\dfrac{\cos \alpha}{\mu} \dfrac{C_{P_c}}{C_T}$ may be determined from the climb angle γ and the

parasite-drag parameter $\dfrac{C_{P_p}}{C_T} \dfrac{\cos \alpha}{\mu}$.

OUTLINE OF PERFORMANCE METHOD UTILIZING CHARTS

The problem of computing helicopter performance may be thought of as finding the value of one variable for given values of other pertinent variables, the variables being related by a number of basic equations. The problem, in essence, thus becomes the solution of a number of simultaneous equations. The procedure can be greatly simplified by utilizing the performance charts presented in figures 2 to 4. The steps required in two typical types of performance calculations will be outlined and demonstrated by a sample calculation.

Calculation of Rate-of-Climb Curves

If the rate of climb (or descent) is required, the calculating procedure would be as follows (for a given μ) for the known parameters P, W, σ, f, ΩR, and ρ:

(1) Assume $T \approx W$ and calculate C_T.

(2) Compute C_P/C_T from equation (5).

(3) Find C_{P_0}/C_T and $\theta_{.75}$ from figure 3.

(4) Find λ from figure 2.

(5) Calculate α from equation (10).

(6) Compute C_{P_i}/C_T amd C_{P_p}/C_T from equations (7) and (8).

(7) Compute C_{P_c}/C_T from equation (2).

(8) Find γ from figure 4.

(9) Compute V_v from the relationship $V_v = V \sin \gamma$.

(10) If both γ and D_p are very large, a new C_T can be computed by means of equation (4) and the process repeated to find a new value of V_v.

Calculation of Power-Required Curves

A common performance calculation is to find the power required by a helicopter flying at a given airspeed and at a given rate of climb (or climb angle). The procedure would be as follows for the known parameters W, σ, f, γ, ΩR, ρ, and V:

(1) Assume that $\alpha = 0^{\circ}$ and that $(\lambda/\mu)^2 \ll 1$; then, calculate T (and C_T) from equation (4).

(2) Calculate μ from its definition.

(3) Calculate C_{P_i}/C_T, C_{P_p}/C_T, and C_{P_c}/C_T from equations (7), (8), and (9), respectively. For convenience of application equation (9) has been used to construct figure 4, from which can be obtained, for example, values of C_{P_c}/C_T for given values of γ and C_{P_p}/C_T.

(4) On the appropriate chart of figure 3, lay off the sum of C_{P_i}/C_T, C_{P_p}/C_T, and C_{P_c}/C_T along the C_P/C_T axis. Then, with that point as a base, construct a line having a slope of unity. (If C_{P_o}/C_T and C_P/C_T were drawn to the same scale in figure 3, the construction line would be drawn at a 45° angle. For the actual scales of figure 3, the line is constructed at an angle which has a tangent of 2.) The intersection of this line with the proper $2C_T/\sigma a$ line will yield values for C_{P_o}/C_T,

C_P/C_T, and $\theta_{.75}$. This procedure is illustrated for a constant tip-speed ratio by the following sketch:

In order to avoid interpolation between tip-speed-ratio charts, the value of V can be chosen so that μ is an even multiple of 0.05; otherwise, the answer can be linearly interpolated between two successive charts.

(5) Since $2C_T/\sigma a$, $\theta_{.75}$, and μ are now known, λ can be found from figure 2.

(6) Compute α from equation (10) and recompute μ from the equation $\mu = \dfrac{V \cos \alpha}{\Omega R}$.

(7) Recompute C_T, C_{P_i}/C_T, C_{P_p}/C_T, and C_{P_c}/C_T and find new values of C_P/C_T and C_{P_o}/C_T. If these values differ from the initially computed ones by more than a few percent, repeat the process. Normally one iteration is sufficient. However, when α is within the range of $\pm 20^\circ$ and $\mu \leqq 0.50$, the initial assumptions that $\cos \alpha = 1$ and $(\lambda/\mu)^2 \ll 1$ are adequate and no iterations are needed.

Sample Performance Calculation

The performance calculations outlined in the preceding section will be illustrated by a sample problem: Calculate the power required by a helicopter traveling at 180 feet per second and climbing at a rate of 300 feet per minute. The following additional data are known: $W = 4,287$ pounds, $\sigma = 0.08$, $\Omega R = 600$ feet per second, $\rho = 0.00238$ slugs per cubic foot, $R = 20$ feet, $\theta_1 = -8°$, and $f = 12$ square feet.

(1) Assume that $\alpha = 0°$ and $(\lambda/\mu)^2 \ll 1$. Also,

$\gamma = \sin^{-1}\dfrac{V_v}{V} = \sin^{-1}\dfrac{5}{180} = 1.6°$ and $D_p = \dfrac{f\rho V^2}{2} = 463$ pounds. Then, from equation (4), $T = 4,300$ pounds, and $C_T = 0.0040$.

(2) Then, $\mu = 180\big/600 = 0.30$.

(3a) From equation (7), $C_{P_i}/C_T = 0.0067$.

(3b) From equation (8), $C_{P_p}/C_T = 0.0322$.

(3c) Then, $\dfrac{\cos \alpha}{\mu}\dfrac{C_{P_p}}{C_T} = 0.107$. From figure 4, $\dfrac{\cos \alpha}{\mu}\dfrac{C_{P_c}}{C_T} = 0.028$.

Thus, $\dfrac{C_{P_c}}{C_T} = 0.0084$.

(4a) $\dfrac{C_{P_i}}{C_T} + \dfrac{C_{P_p}}{C_T} + \dfrac{C_{P_c}}{C_T} = 0.0067 + 0.0322 + 0.0084 = 0.0473.$

(4b) For $\mu = 0.30$ and $2C_T/\sigma a = 0.018$, figure 3(e) gives:

$$\frac{C_{P_o}}{C_T} = 0.0315$$

$$\frac{C_P}{C_T} = 0.0788$$

$$\theta_{.75} = 9°$$

(5) For $\theta_{.75} = 9°$ and $2C_T/\sigma a = 0.018$, figure 2(e) gives $\lambda = -0.080$.

(6) The rotor angle of attack α can now be computed from equation (10) as follows:

$$\tan \alpha = \frac{-0.080}{0.30} + \frac{0.004}{0.18(1 + 0.0712)^{1/2}} = -0.245$$

$$\alpha = -13.8°$$

(7a) Recomputing the power coefficients with the above values for α and λ results in changes that are within the accuracy of the computations; therefore, the originally computed values are sufficient.

(7b) The power required is then calculated as

$$\text{Power} = \frac{C_P}{C_T} C_T \pi R^2 \rho (\Omega R)^3$$

$$= (0.079)(0.004)\pi(20)^2(0.00238)(600)^3$$

$$= 204,000 \text{ ft-lb/sec}$$

$$= 371 \text{ hp}$$

(7c) The rotor profile-drag power is

$$\text{Profile power} = \frac{0.031}{0.079} \times 204,000$$

$$= 80,000 \text{ ft-lb/sec}$$

$$= 146 \text{ hp}$$

RANGE OF APPLICATION OF CHARTS

In the preparation of the charts, it was necessary to make some assumptions regarding the rotor physical parameters to be used with the theory. Some of the more pertinent effects of these assumptions as well as the effects of the restrictive assumptions of the theory are discussed in the succeeding sections.

Blade Characteristics

The sample rotor for which the charts presented herein were prepared was assumed to have hinged rectangular blades with a mass factor $\rho c a R^4/I_1$ equal to 15 and a linear twist of -8°. However, according to the error analysis made in reference 6, it would appear that the charts would be applicable to rotors having values of mass factors ranging from 0 to 25. Thus, although blade-flapping motion is sensitive to mass factor, average rotor forces are relatively insensitive to moderate changes in the flapping motion.

Although the charts were calculated for rotors having uniform-chord blades, previous experience has shown that, in general, the forward-flight performance of rotors with blades having as much as 3:1 taper ratio can be predicted with good accuracy by equations derived for uniform-chord blades, provided that the rotor solidity is based on the equivalent weighted chord c_e.

In order to investigate the applicability of the charts to rotors with blades having values of twist other than -8°, the theoretical values of C_{P_O}/C_T for values of twist equal to 0°, -8°, and -16° were compared at several unstalled flight conditions. From the comparison, it appeared that for forward speeds ranging from the speed for minimum power to the maximum speeds of present-day helicopters (that is, for values of tip-speed ratio between approximately 0.05 and 0.30) the effects of twist on the profile power are small, particularly when considered as a percentage of the total power required. The importance of twist, however, is not primarily its effect on profile power but in the delay of stall. The effect of twist on stall limits is discussed in a later section of this paper.

Airfoil Section Characteristics

The three-term drag polar used in the preparation of the charts (see section entitled "Method of Analysis") is considered as representative of practical construction blades of conventional airfoil section having fairly accurate leading-edge profiles and rigid surfaces. The charts may be applied, however, to rough or poorly built blades of conventional section by multiplying the profile-drag—thrust ratio obtained from the charts by a constant "roughness" factor equal to the ratio of the average of the ordinates of the drag curve of the actual blade to the average of the ordinates of the drag curve used in the charts. If the drag curves do not have similar shapes, the determination of this factor should take into account the relative importance of different angles of attack; a basis for doing this by a method of "weighting" curves is discussed in reference 7. The angle of attack at which stall occurs will also be affected by the roughness of the blade surface, and consideration should

be given to the surface condition when estimating the limits of validity
of the theory.

Stall Limits

Satisfactory limits to the use of a theory in which stall is not
considered are, for powered flight, the conditions at which the tip of
the retreating blade reaches its stalling angle of attack, as shown in
references 2 and 6. For the autorotative case, limits to the theory are
shown to consist of the conditions at which the velocity of the blade
elements of the stalled inboard sections reach high enough values so that
the contributions of these elements to the total thrust and torque of the
rotor become significant. Therefore, following the procedure of previous
NACA rotor papers (such as ref. 2), there are included on the charts of
this paper two sets of limit lines. One set corresponds to conditions at
which a blade element at an aximuth angle of 270° with a relative velocity
equal to 0.4 of the tip speed reaches angles of attack of 12° and 16°,
whereas the other set corresponds to conditions at which the blade tip
at an azimuth angle of 270° reaches angles of attack of 12° and 16°.
These limit lines are designated by the symbols $\alpha_{\left(u_T = 0.4\right)\left(270^\circ\right)}$

and $\alpha_{(1.0)(270^\circ)}$, respectively. The 12° and 16° lines represent a range
of angles of attack in which conventional blade airfoils would be expected
to stall. Also, since vibration and control limitations brought on by
blade stall occur, in general, when the calculated stall angle is exceeded
by about 4°, the difference between the 12° and 16° lines should also be
useful in estimating the limits to practical operating conditions of a
rotor. Moderate amounts of stall can be approximately accounted for by
empirical corrections to the profile power when the limit lines on the
charts are exceeded. The basis on which these corrections may be made is
discussed in reference 8 and the procedure is summarized in reference 4
(pp. 266-267).

Theory indicates, and flight measurements have shown, that blade
twist is effective in delaying stall. Twisting the blade so as to lower
the pitch at the tip with respect to the pitch at the root tends to dis-
tribute the lift more evenly along the blades and therefore minimizes the
high angles of attack in the tip region. Combinations of C_P/C_T
and $2C_T/\sigma a$ for which blade angles of attack at the specified station
reach 12° and 16° for 0°, -8°, and -16° twist are plotted in figure 5.
As would be expected, these plots show that higher values of C_T/σ can
be attained with negative twist before retreating blade stall is encoun-
tered. Conversely, the greater the negative twist, the higher the tip-
speed ratio that can be reached at a given C_T/σ before the onset of
stall.

It should be noted that negative values of twist tend to decrease the angle of attack at the tip of the advancing blade. The advancing-blade-tip angle of attack is shown in figure 6 as a function of $2C_T/\sigma a$ and μ at several power conditions (as represented by the pitch values) for twists of -8° and -16°. Although the large negative angles of attack at the advancing-blade tip will adversely affect the performance, this effect is believed to be of less importance than the benefits achieved by the delay in retreating blade stall. There is the possibility, however, that high negative advancing-blade-tip angles of attack would result in a contribution to blade stresses which should be considered for individual designs. It should be noted, however, that these tip angles were calculated on the basis of uniform inflow velocity, and the local upwash which tends to occur at the advancing tip should result in less negative values.

Compressibility Limits

The section lift and drag coefficients used in the preparation of the charts of this paper do not vary with Mach number. It is expected that the primary effect of such variation would be an increase in the profile-drag power if the drag-divergence Mach number were approached or exceeded. Therefore, the charts underestimate the power required for a rotor operating within the range where compressibility effects are encountered. It is hoped that power losses due to compressibility may be taken into account by adding corrections to the charts in a manner similar to that done for the effects of stall. The corrections probably could be based on results of strip analyses or on experimental data. The operational limits imposed by Mach number, however, are yet to be determined.

CONCLUDING REMARKS

Charts based on rotor theory have been presented from which the profile-drag—thrust ratio of a rotor can be determined for various combinations of pitch angle, ratio of thrust coefficient to solidity, tip-speed ratio, and power input. The equations on which the charts are based have taken into account blade stall in the reversed-velocity region and are not limited by small-angle assumptions for blade pitch and inflow angles. For these reasons the method is believed to be more accurate than previous methods for cases wherein the rotor inflow velocity is relatively large, for rotors operating at steep rates of climb or descent, for flight at high tip-speed ratios, or for convertiplane transition attitudes.

In addition to providing a convenient means for quickly estimating rotor performance, the charts should be useful as a means for estimating the effects of changes in design variables and as a base to which corrections may be applied for the effects of stall and compressibility. Limit lines which indicate the stall condition of the rotor and which serve to indicate the limits to practical rotor operating conditions are shown in the charts.

The method of using the charts for performance estimation is outlined and illustrated through computation of a sample problem.

Langley Aeronautical Laboratory,
    National Advisory Committee for Aeronautics,
        Langley Field, Va., October 1, 1954.

REFERENCES

1. Gessow, Alfred, and Crim, Almer D.: An Extension of Lifting Rotor Theory To Cover Operation at Large Angles of Attack and High Inflow Conditions. NACA TN 2665, 1952.

2. Bailey, F. J., Jr., and Gustafson, F. B.: Charts for Estimation of the Characteristics of a Helicopter Rotor in Forward Flight. I — Profile Drag-Lift Ratio for Untwisted Rectangular Blades. NACA WR L-110, 1944. (Formerly NACA ACR L4H07.)

3. Pope, Alan: Summary Report of the Forces and Moments Over an NACA 0015 Airfoil Through 180° Angle of Attack. Aero Digest, vol. 58, no. 4, Apr. 1949, pp. 76-78, 100.

4. Gessow, Alfred, and Myers, Garry C., Jr.: Aerodynamics of the Helicopter. The Macmillan Co., c.1952.

5. Gessow, Alfred: An Analysis of the Autorotative Performance of a Helicopter Powered by Rotor-Tip Jet Units. NACA TN 2154, 1950.

6. Bailey, F. J., Jr.: A Simplified Theoretical Method of Determining the Characteristics of a Lifting Rotor in Forward Flight. NACA Rep. 716, 1941.

7. Gustafson, F. B.: Effect on Helicopter Performance of Modifications in Profile-Drag Characteristics of Rotor-Blade Airfoil Sections. NACA WR L-26, 1944. (Formerly NACA ACR L4H05.)

8. Gustafson, F. B., and Gessow, Alfred: Effect of Blade Stalling on the Efficiency of a Helicopter Rotor as Measured in Flight. NACA TN 1250, 1947.
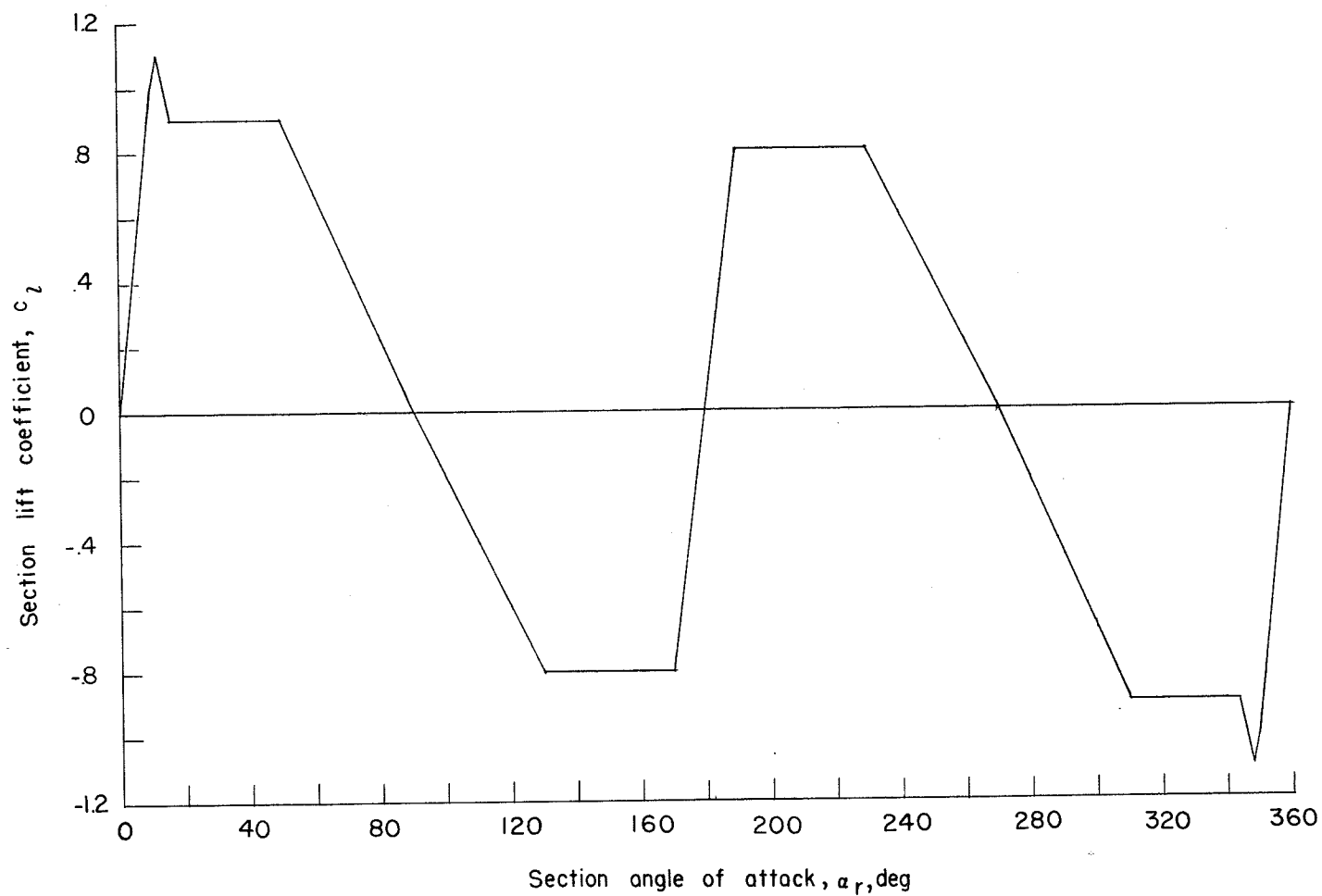
(a) c_l plotted against α_r.

Figure 1.- Section lift and drag characteristics used in evaluation of reversed-velocity region.

$c_{d_0} = 0.02 - 0.0216(\pi - \alpha_r) + 0.4(\pi - \alpha_r)^2$

$c_{d_0} = 0.0087 - 0.0216\alpha_r + 0.4\alpha_r^2$

$c_{d_0} = 0.02 - 0.0216(\alpha_r - \pi) + 0.4(\alpha_r - \pi)^2$

$c_{d_0} = 0.0087 - 0.0216(2\pi - \alpha_r) + 0.4(2\pi - \alpha_r)^2$

Section angle of attack, α_r, deg
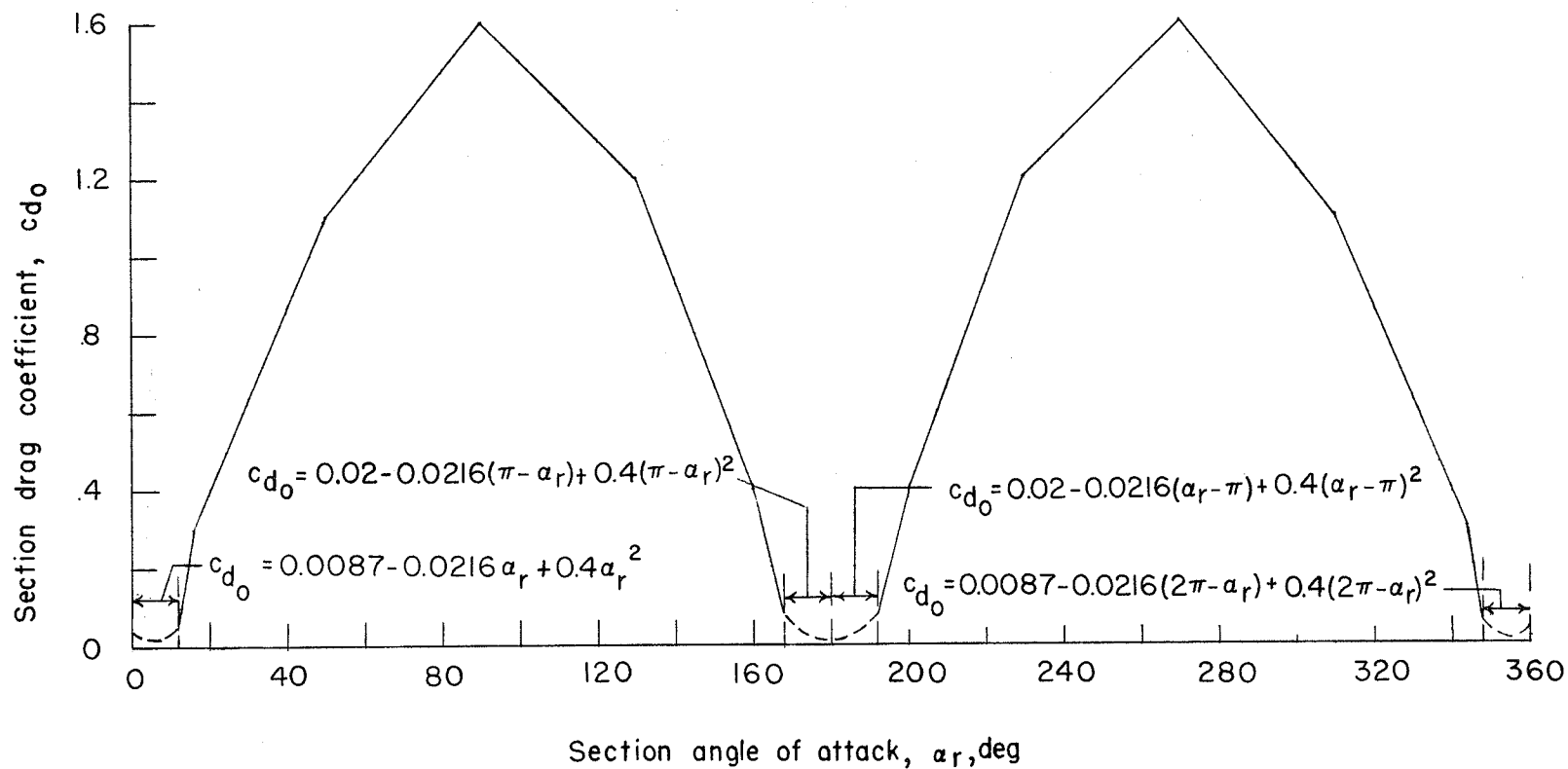
(b) c_{d_0} plotted against α_r.

Figure 1.- Concluded.
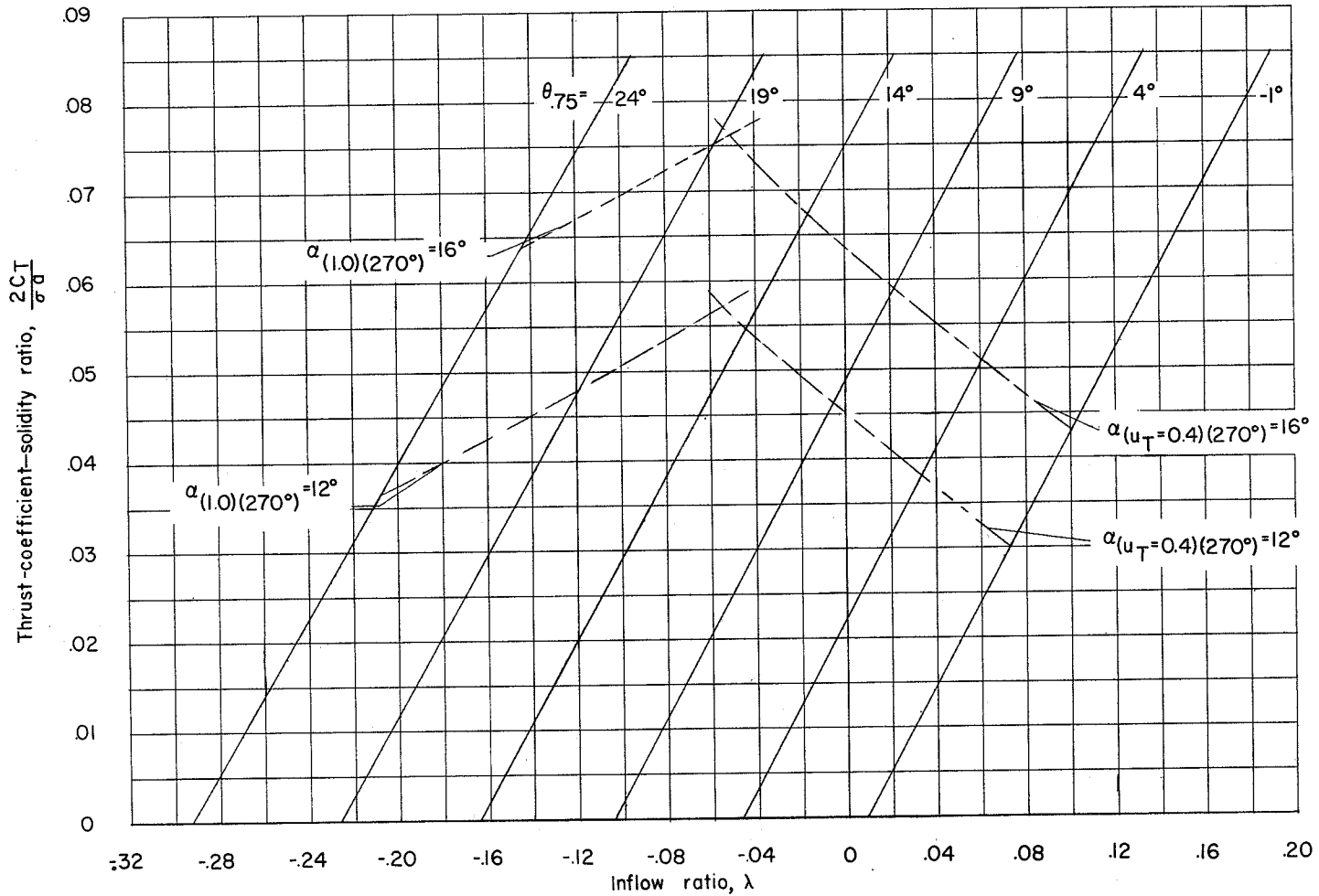
(a) $\mu = 0.05$.

Figure 2.- Thrust-coefficient—solidity ratio plotted against inflow ratio for blades having $-8°$ twist.
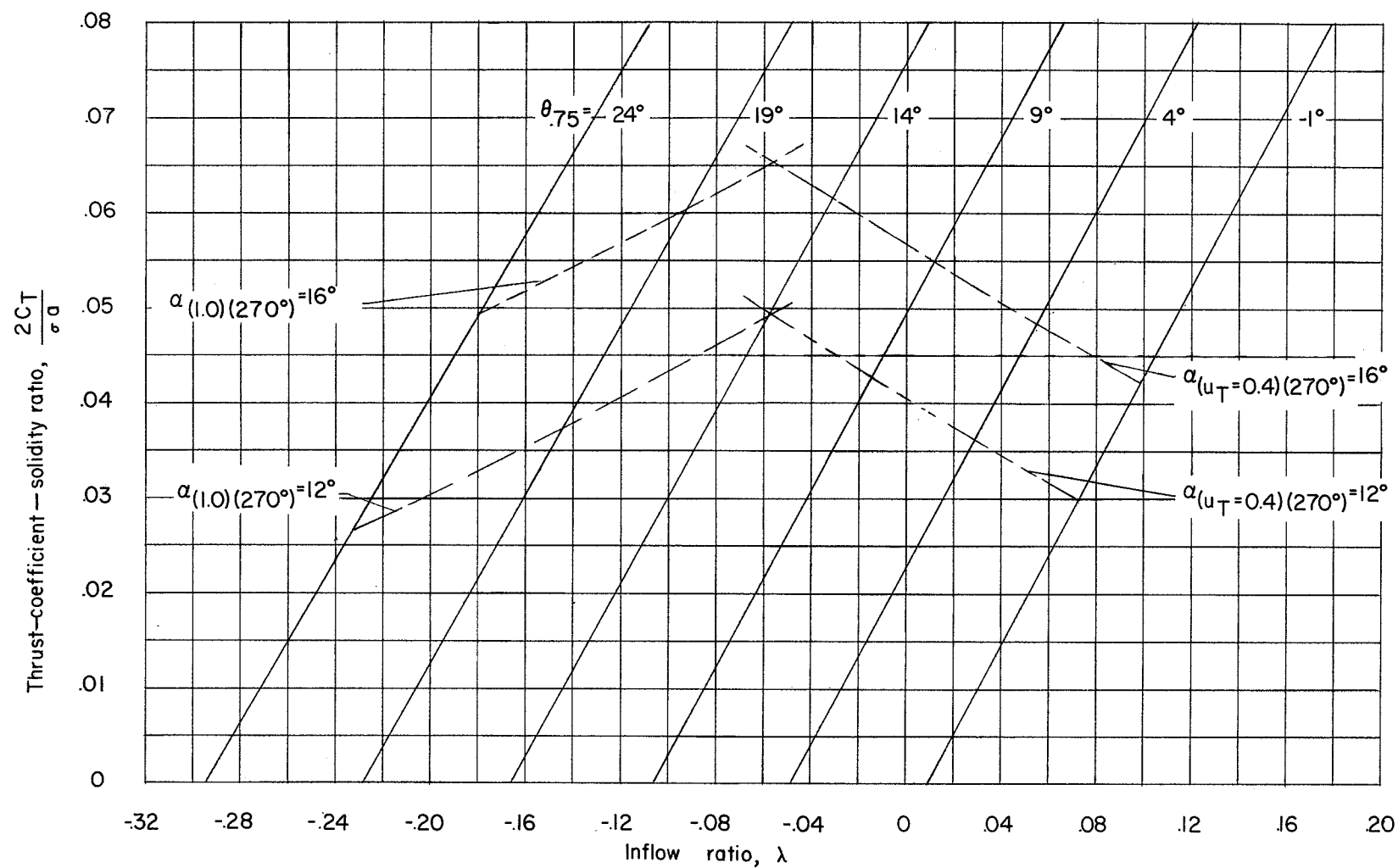
(b) $\mu = 0.10$.

Figure 2.- Continued.
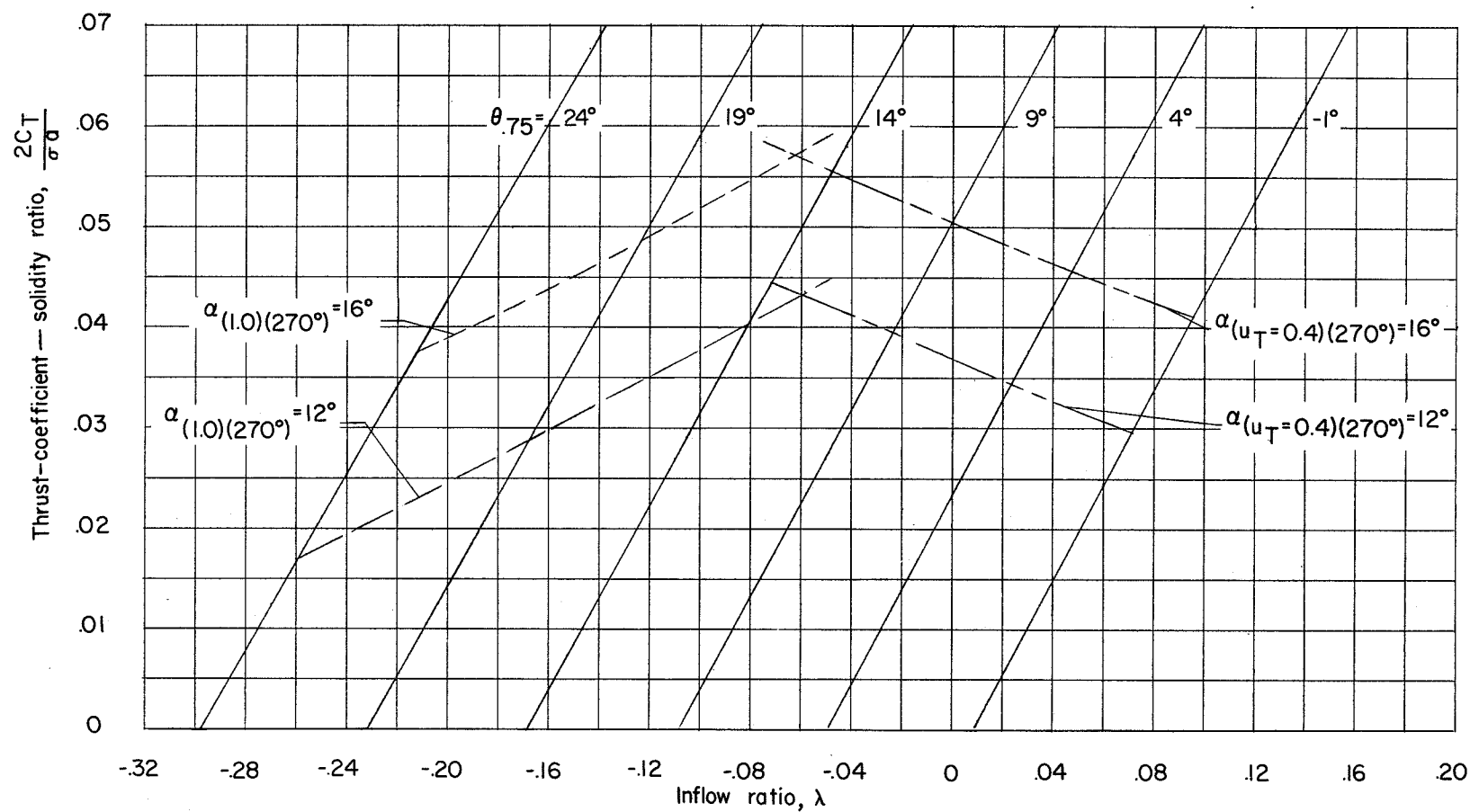
(c) $\mu = 0.15$.

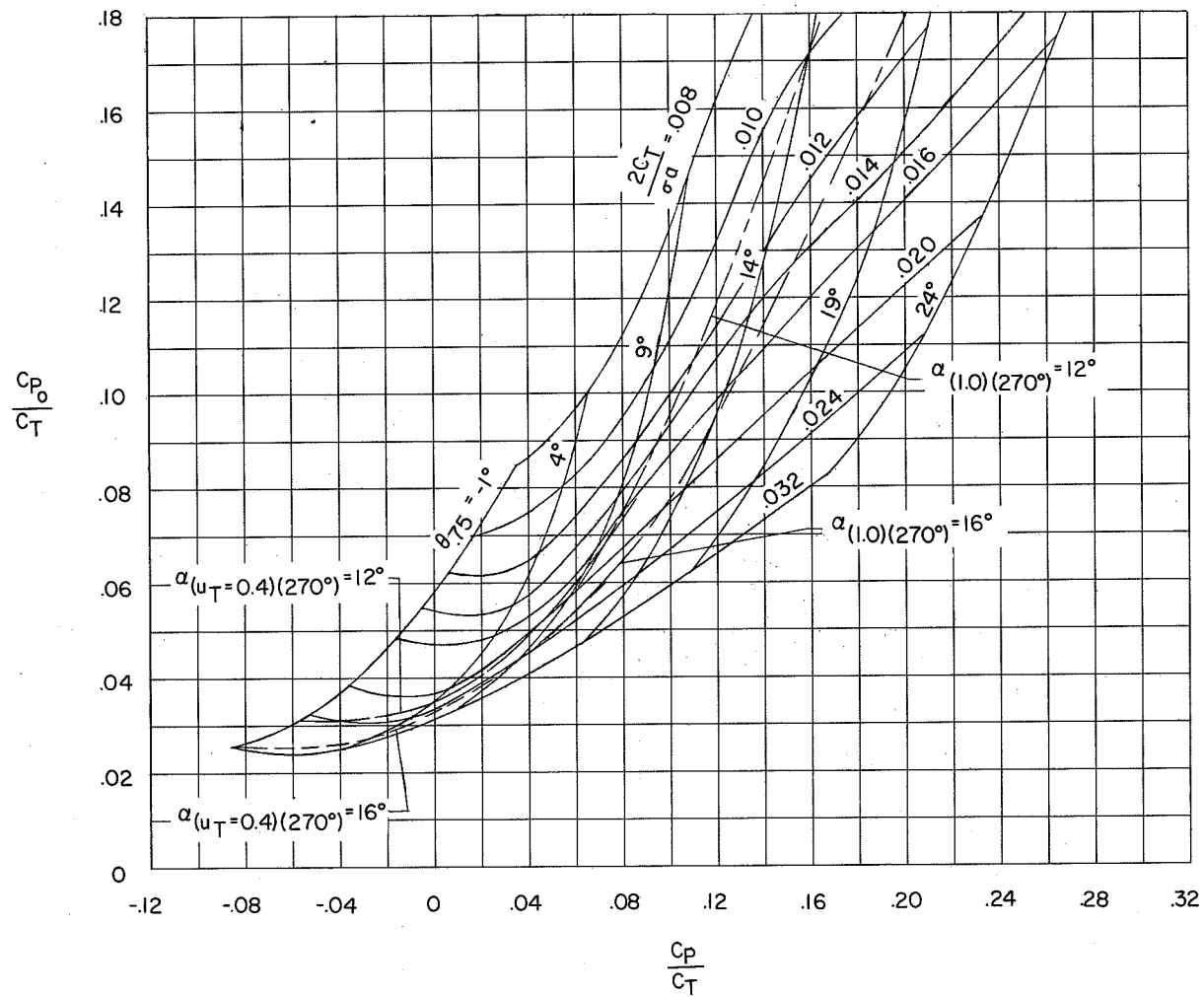Figure 2.- Continued.
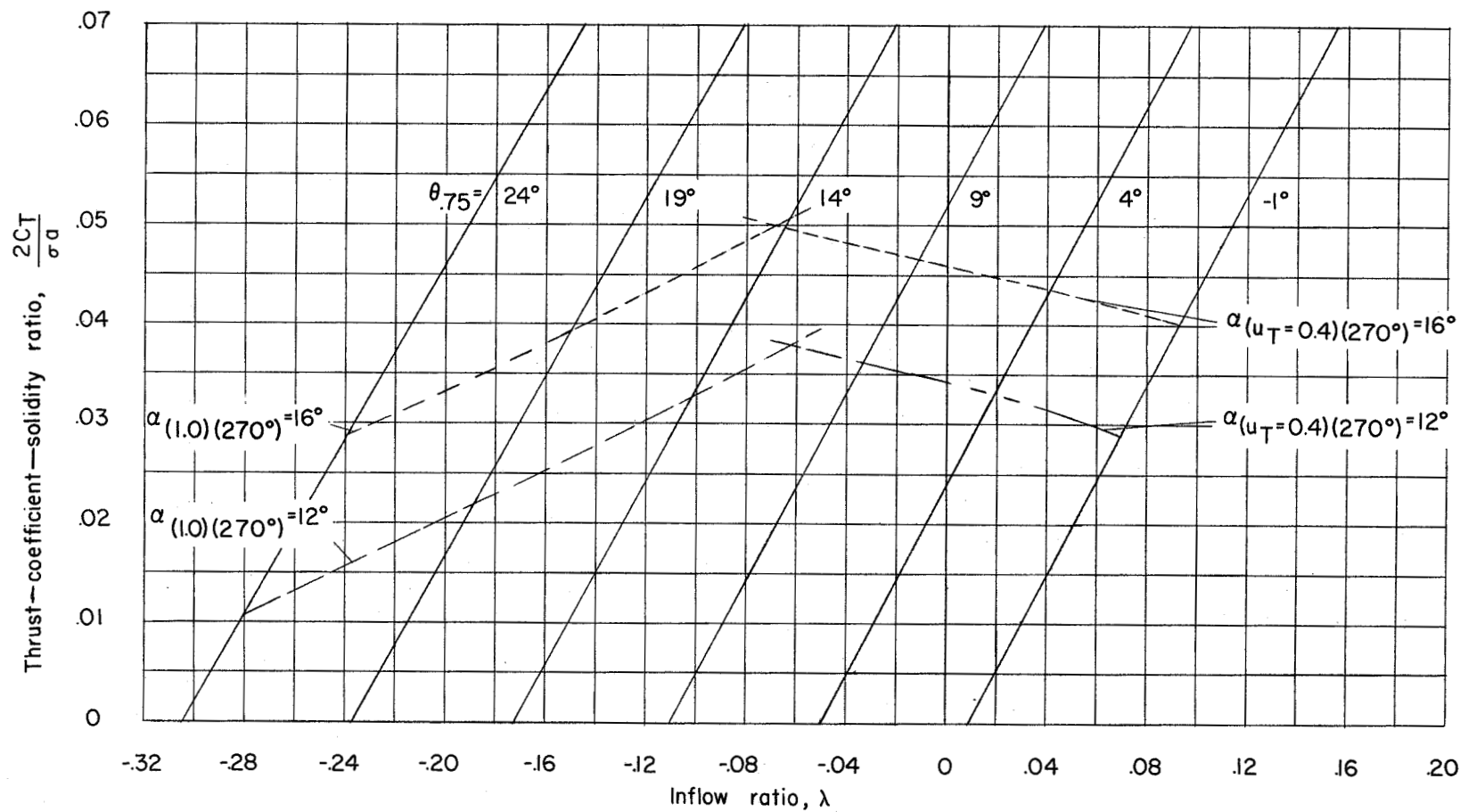
(d) $\mu = 0.20$.

Figure 2.- Continued.
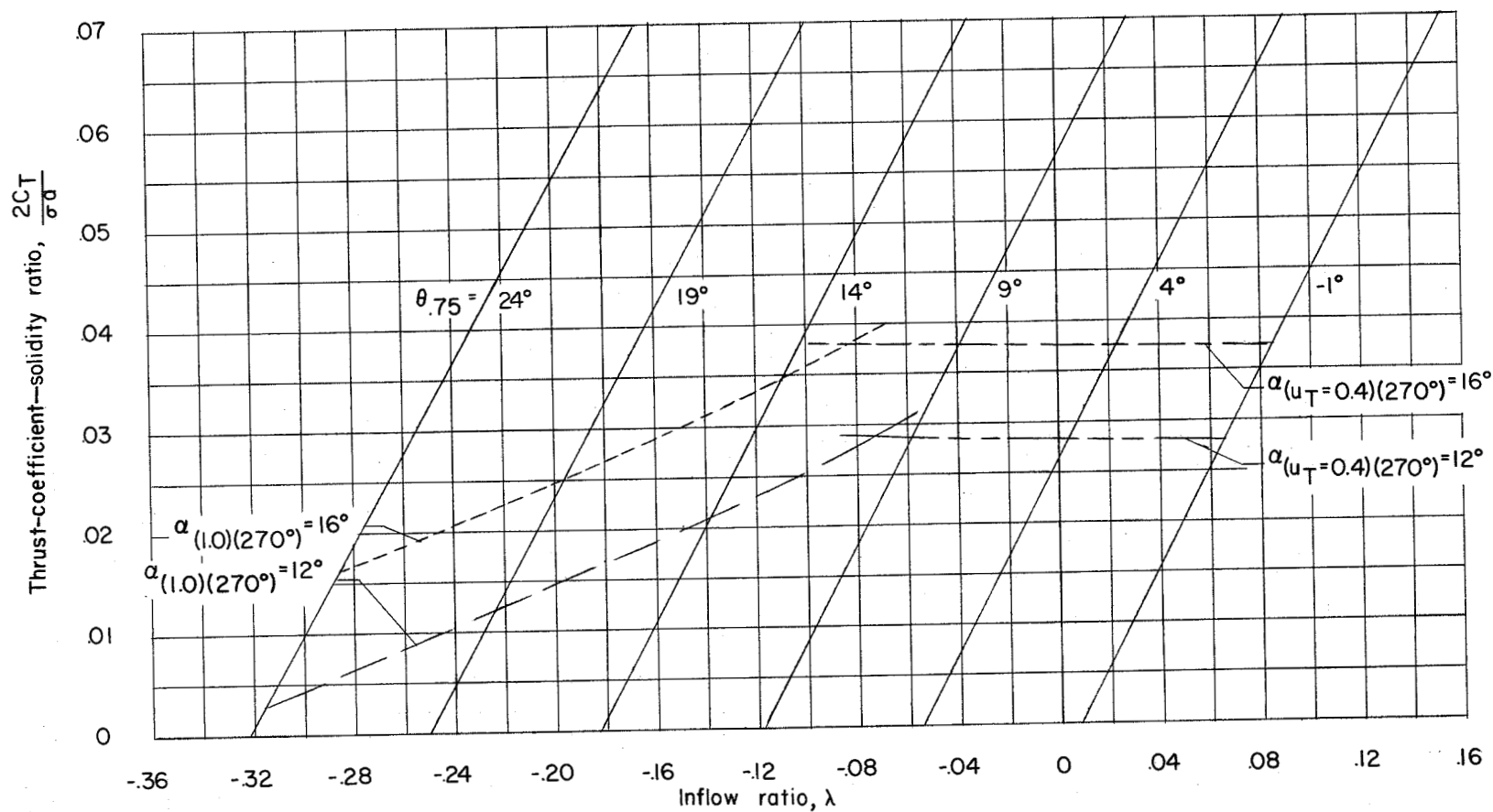
(e) $\mu = 0.30$.

Figure 2.- Continued.
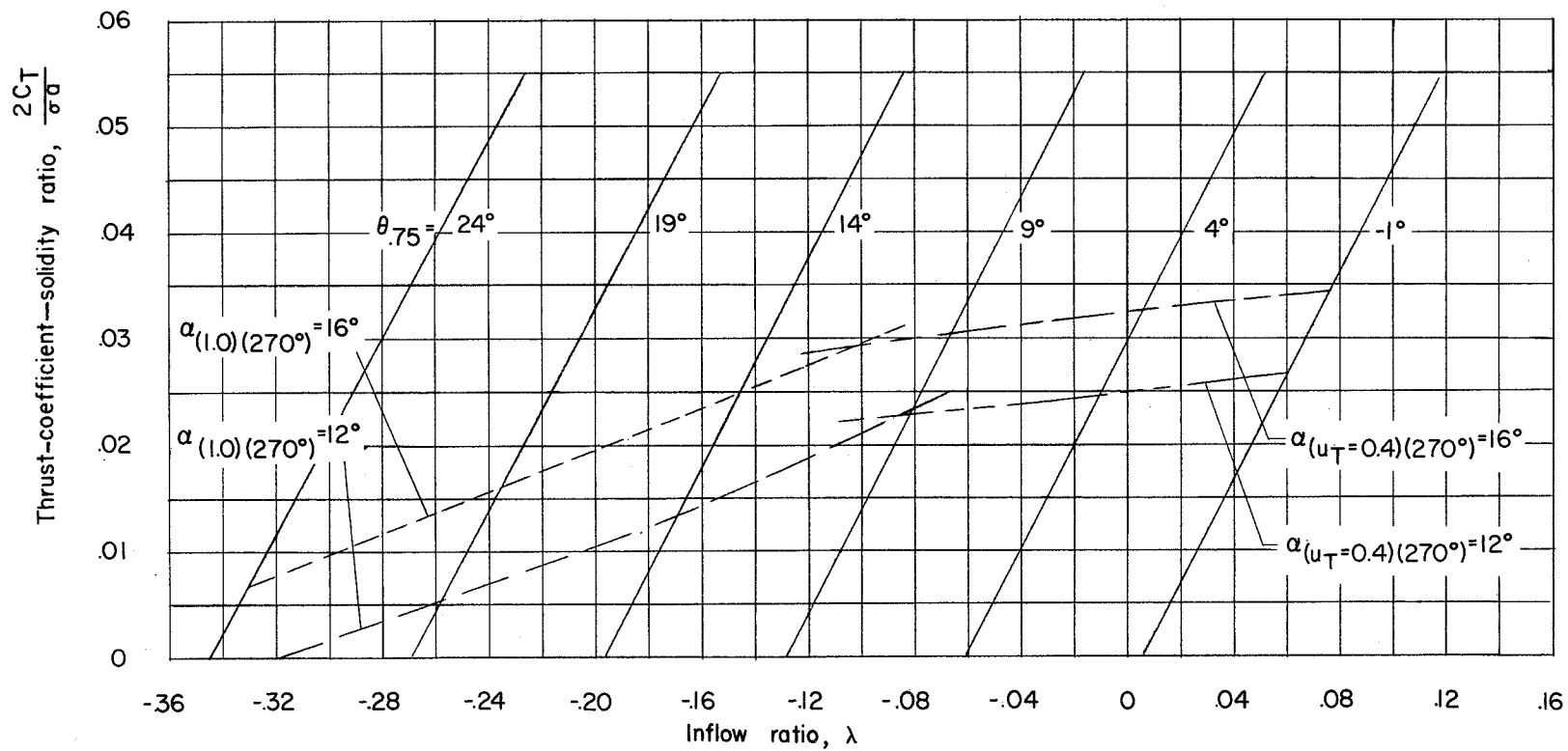
(f) $\mu = 0.40$.

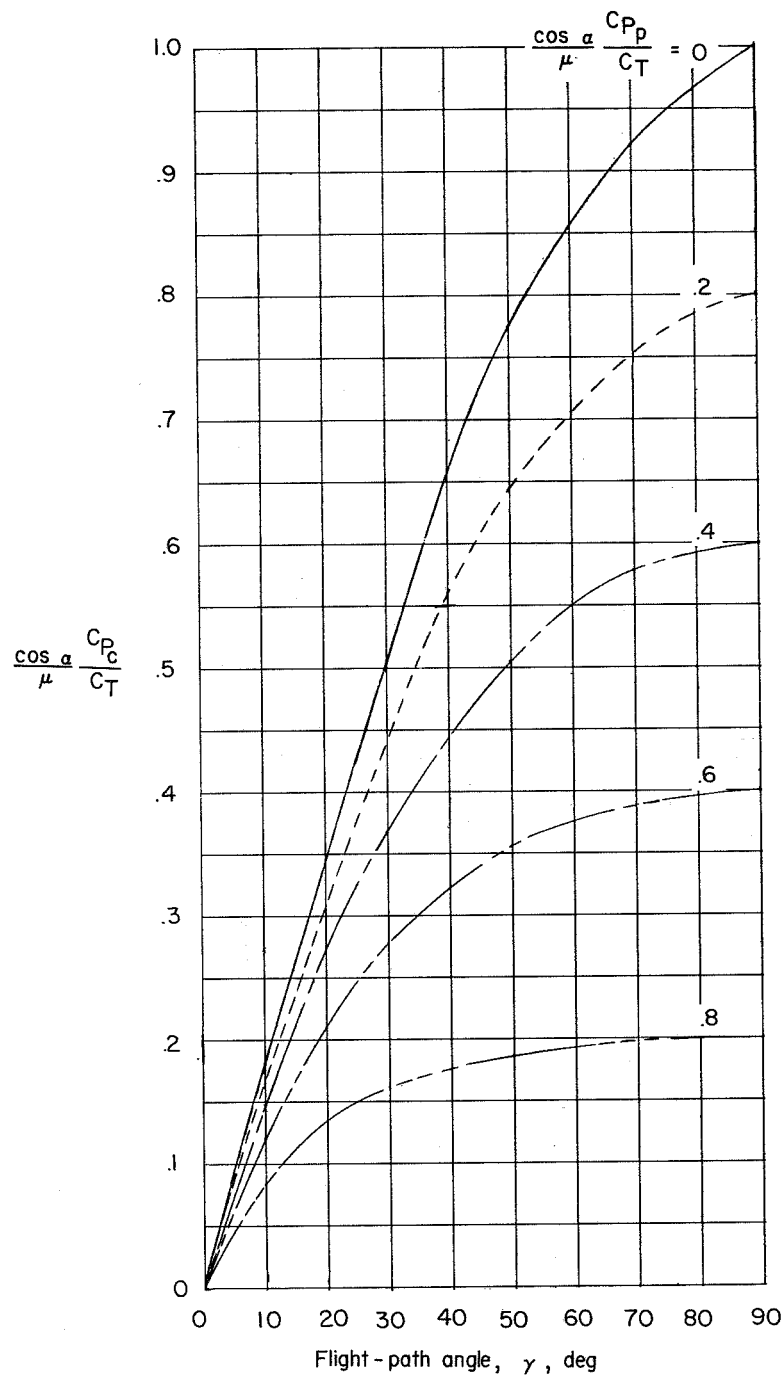Figure 2.- Continued.
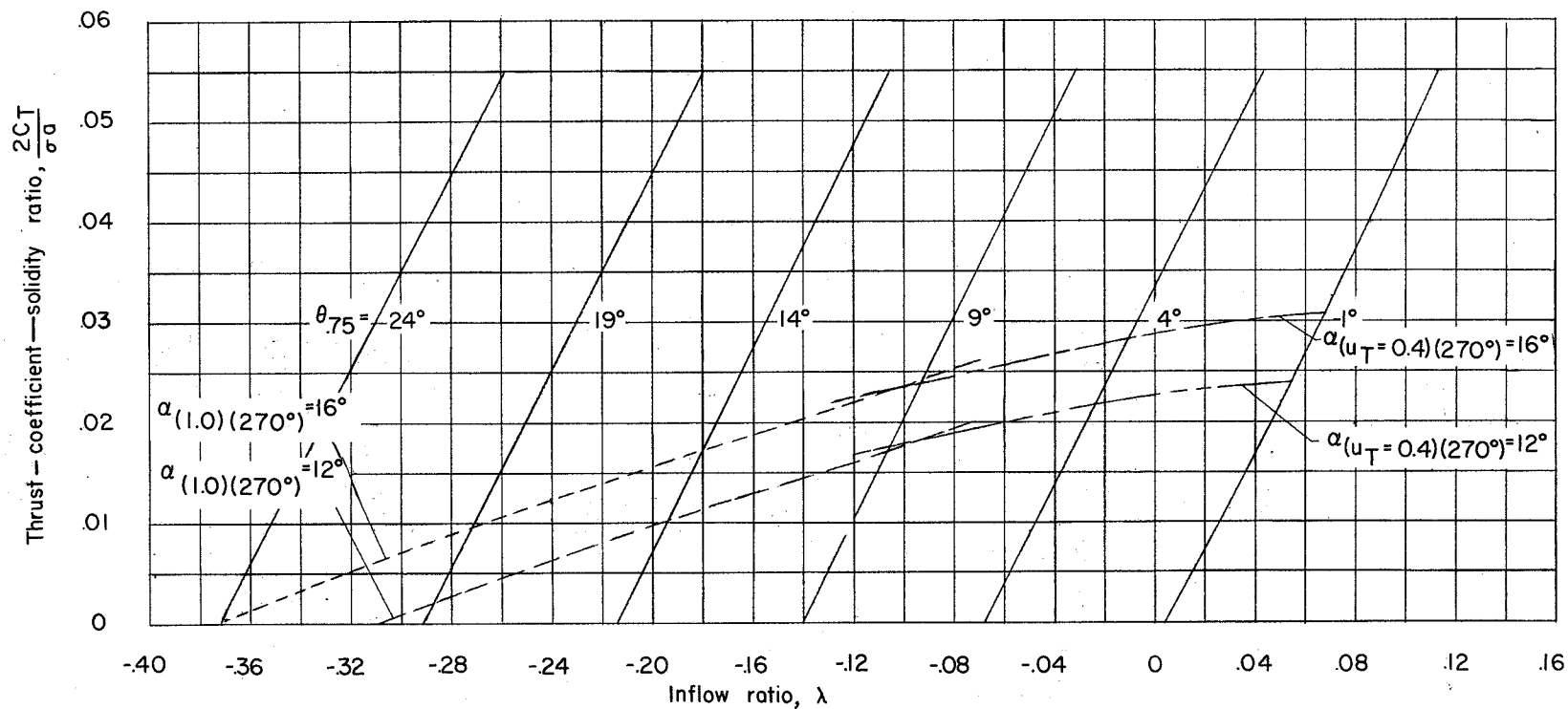
(g) μ = 0.50.

Figure 2.- Concluded.
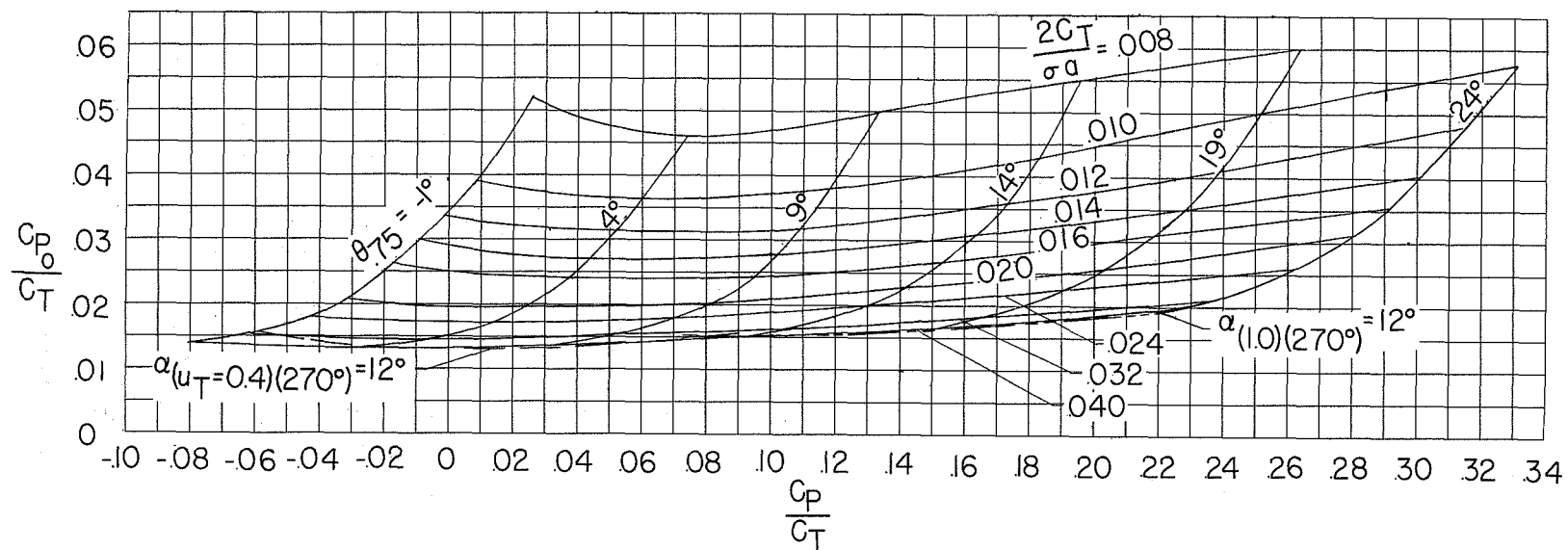
(a) $\mu = 0.05$.

Figure 3.- Profile-drag—thrust ratio for blades having -8° twist.
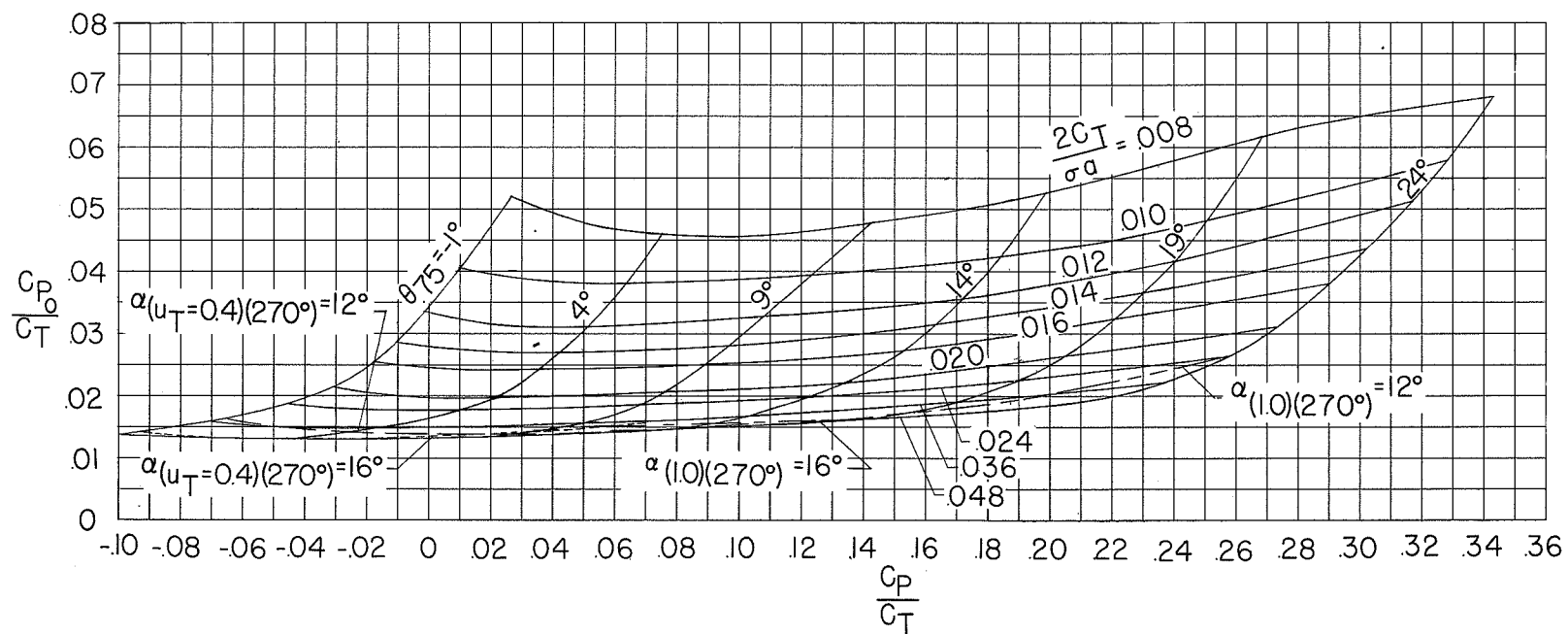
(b) μ = 0.10.

Figure 3.- Continued.
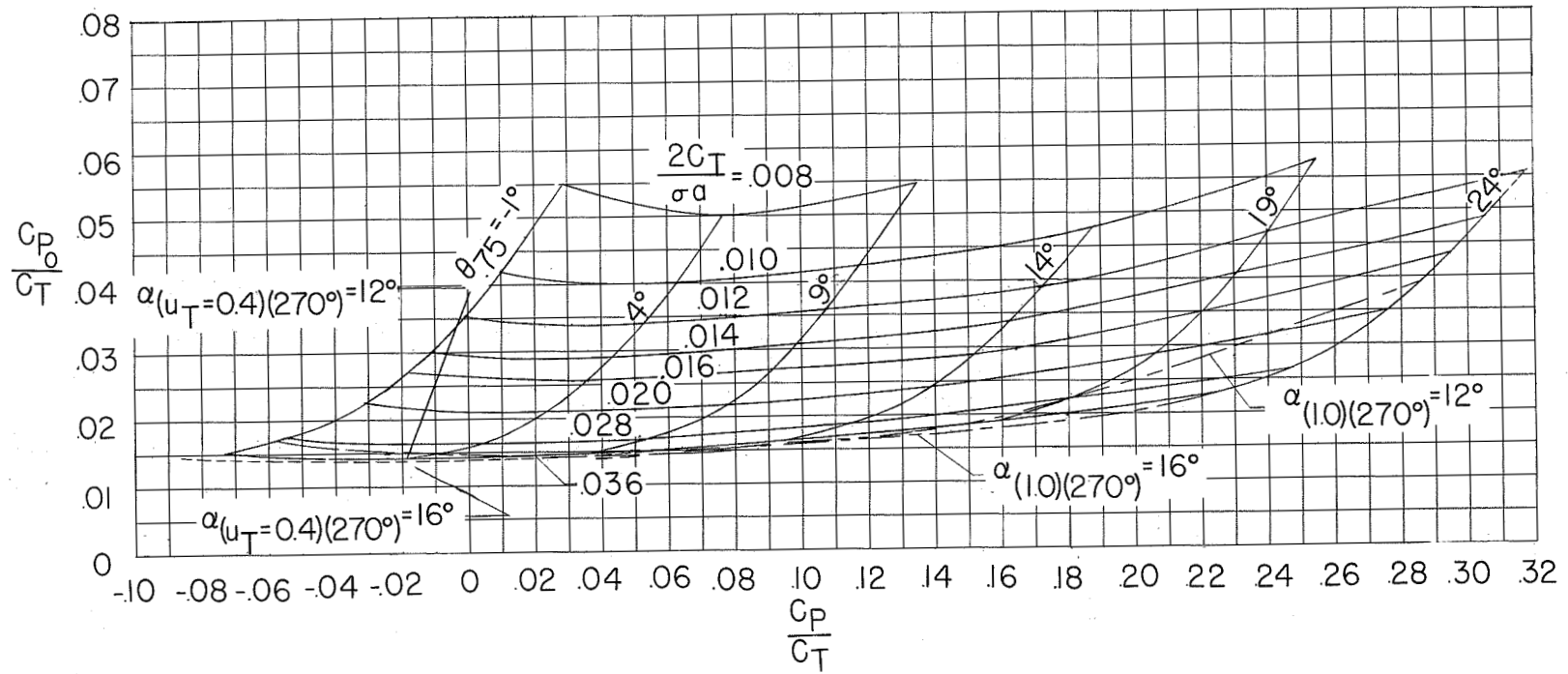
(c) $\mu = 0.15$.

Figure 3.- Continued.
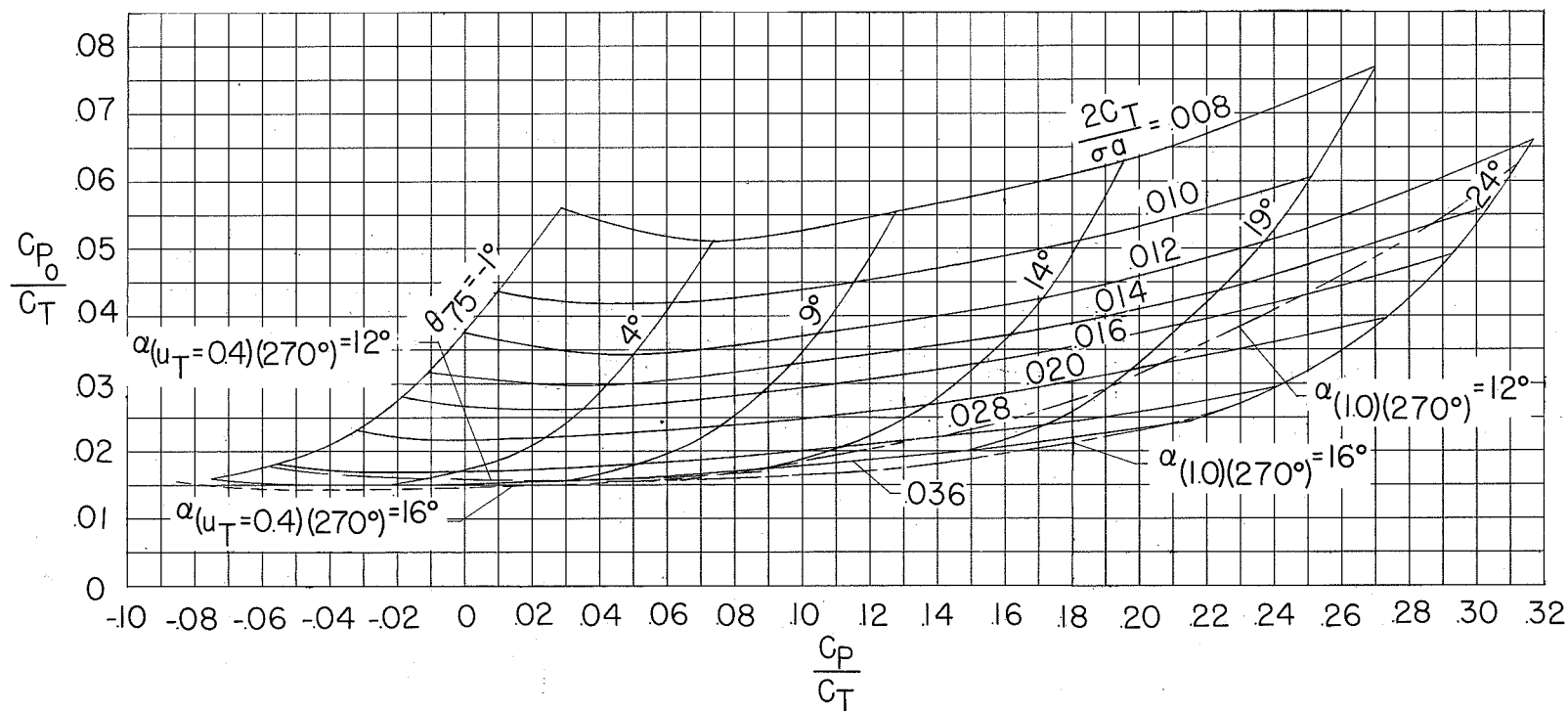
(d) $\mu = 0.20$.

Figure 3.- Continued.
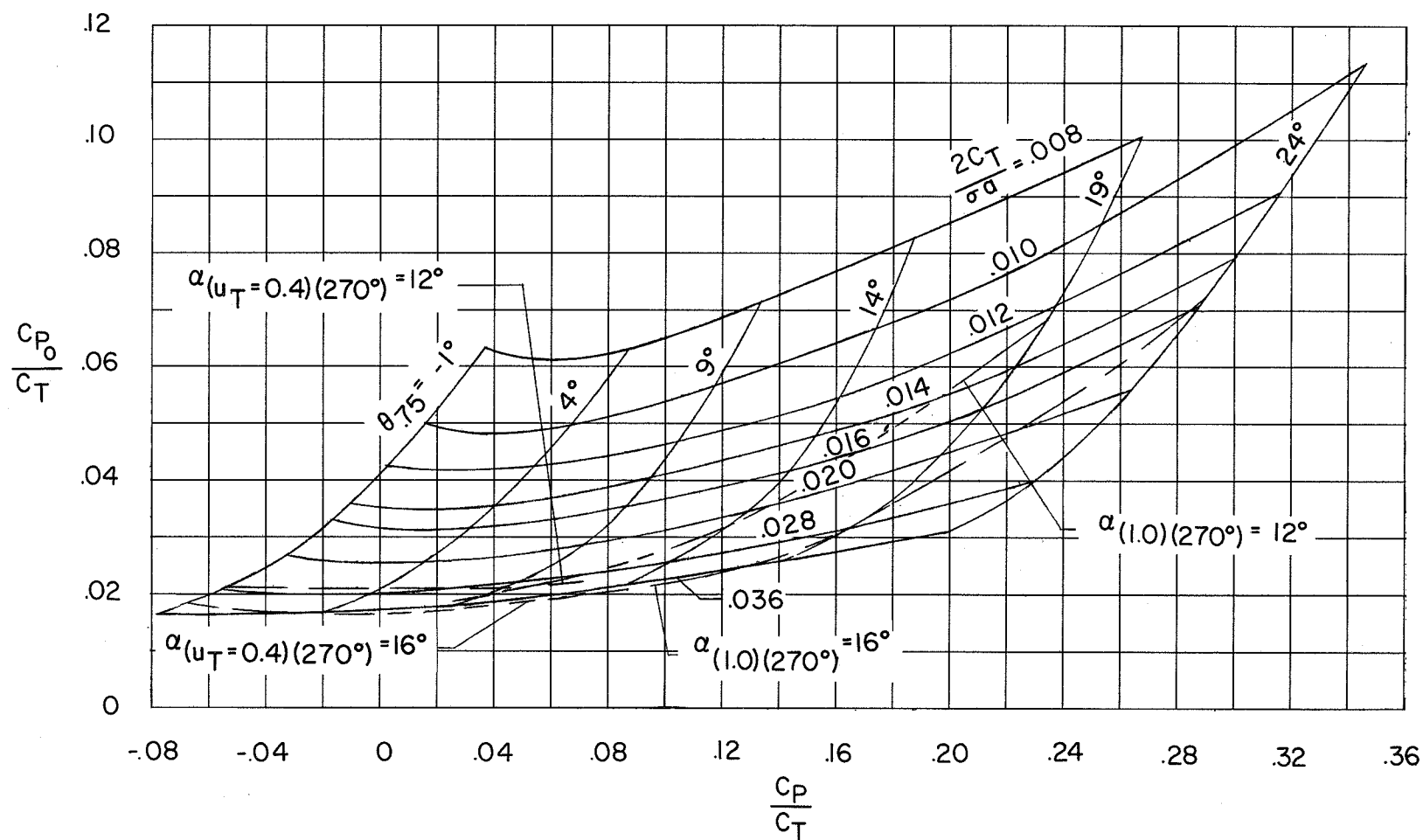
(e) $\mu = 0.30$.

Figure 3.- Continued.
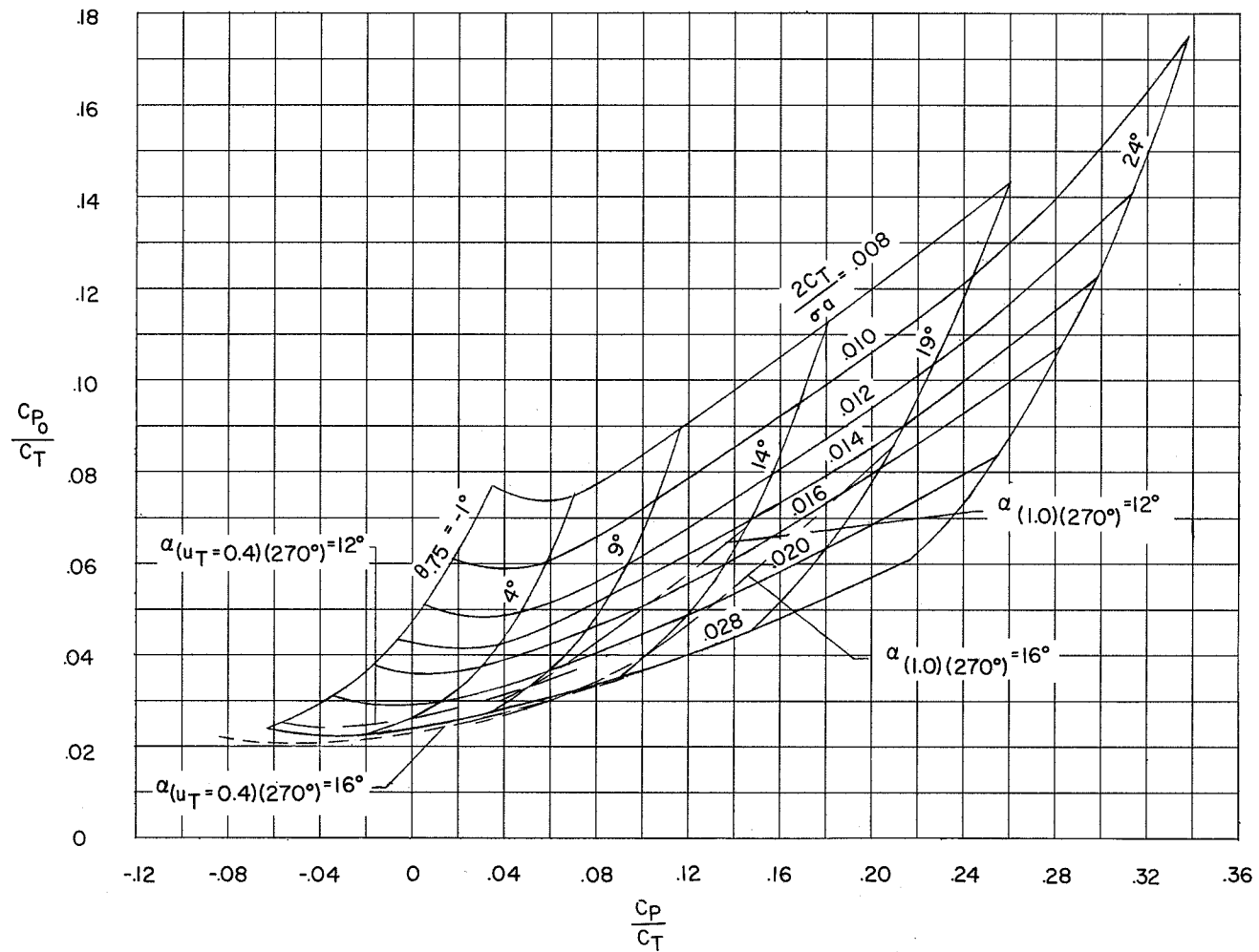
(f) μ = 0.40.

Figure 3.- Continued.

(g) $\mu = 0.50.$

Figure 3.- Concluded.

(a) Climb (γ positive).

Figure 4.- Climb parameter $\dfrac{\cos\,\alpha}{\mu}\,\dfrac{C_{P_c}}{C_T}$ as a function of flight-path angle and parasite-drag parameter.
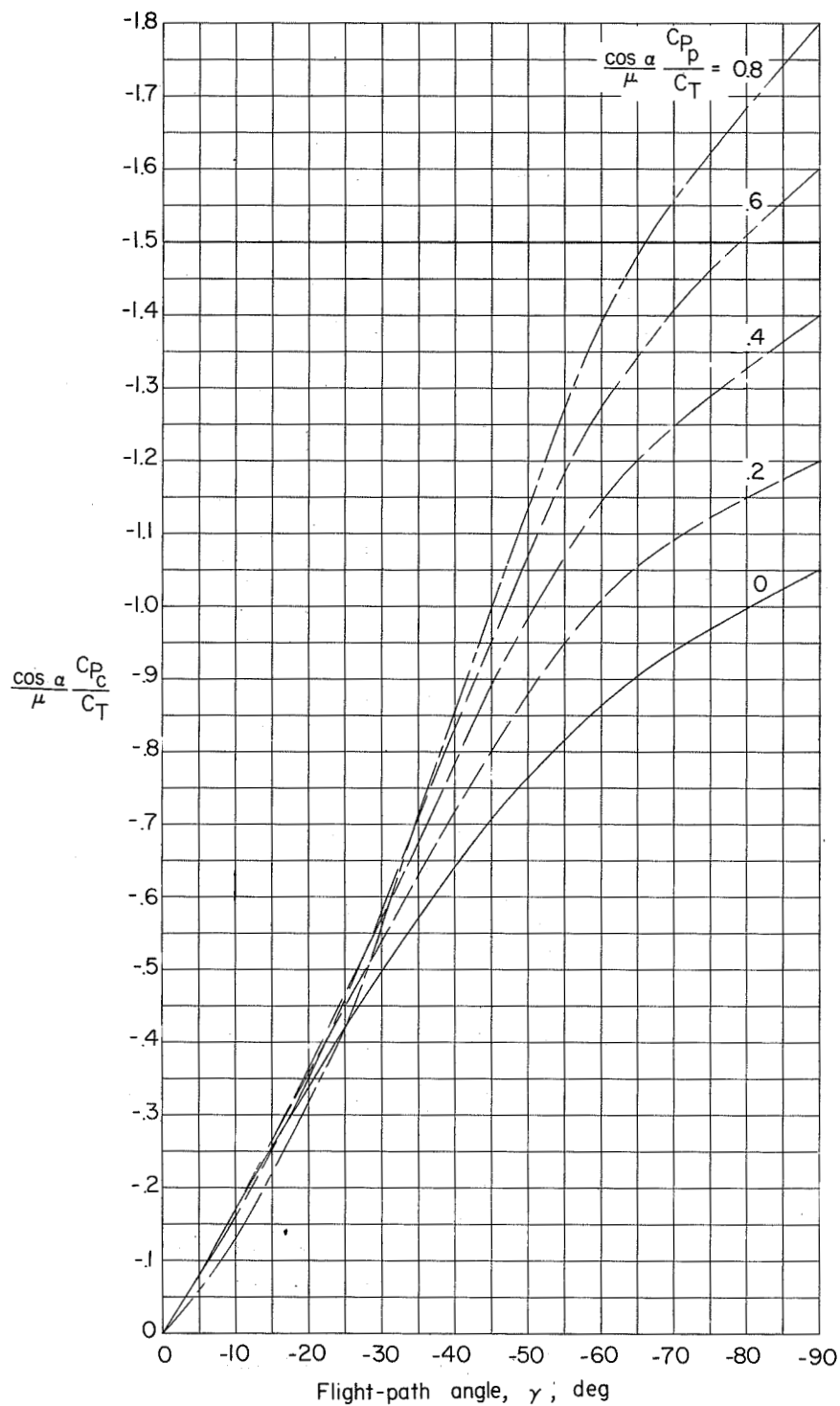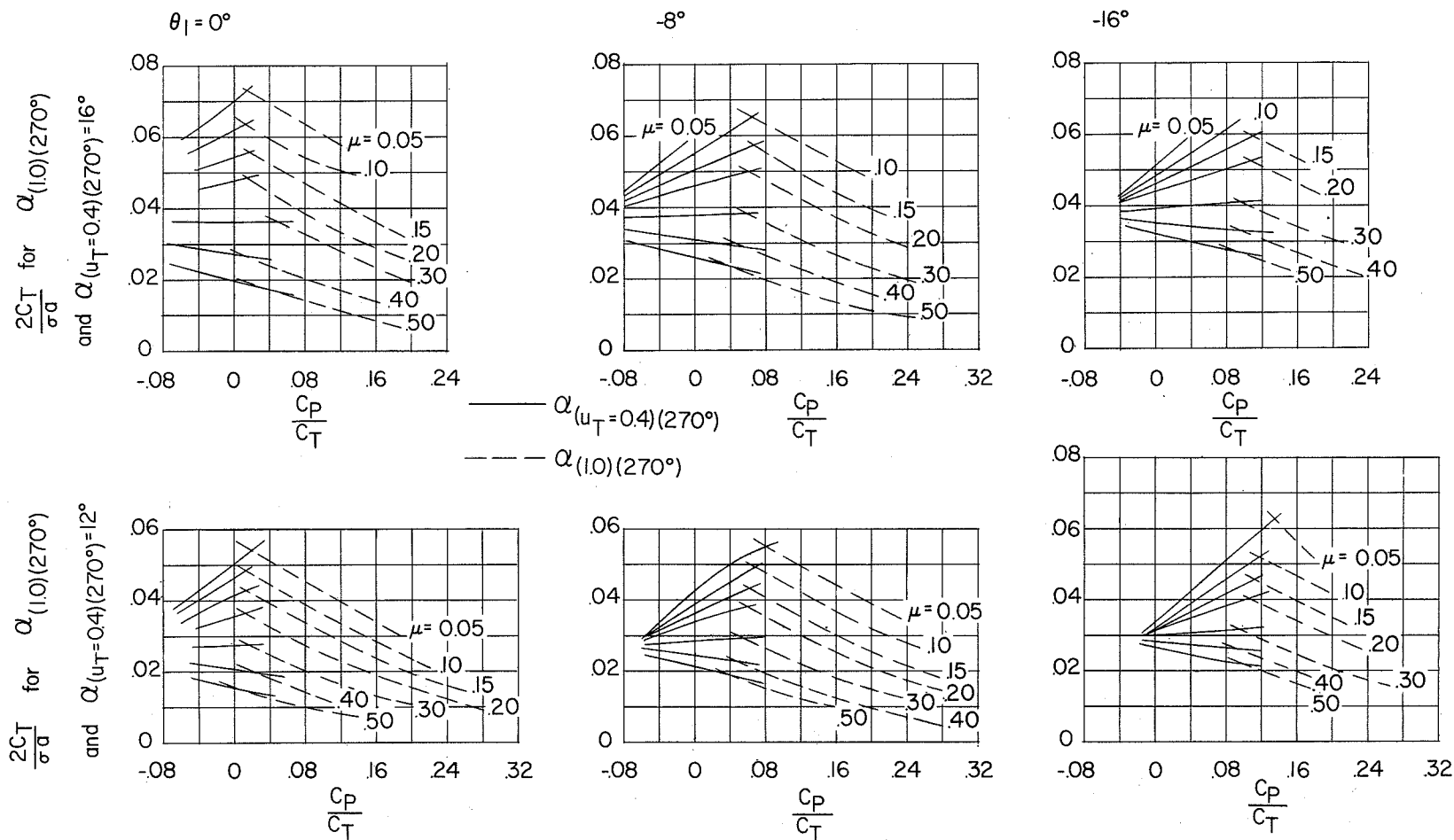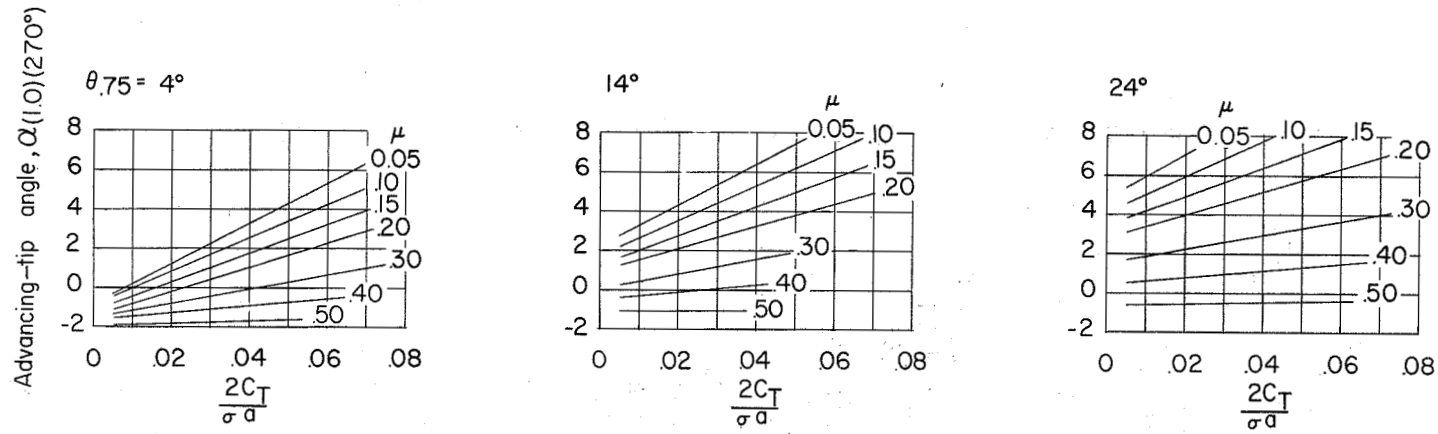
(b) Descent (γ negative).

Figure 4.- Concluded.
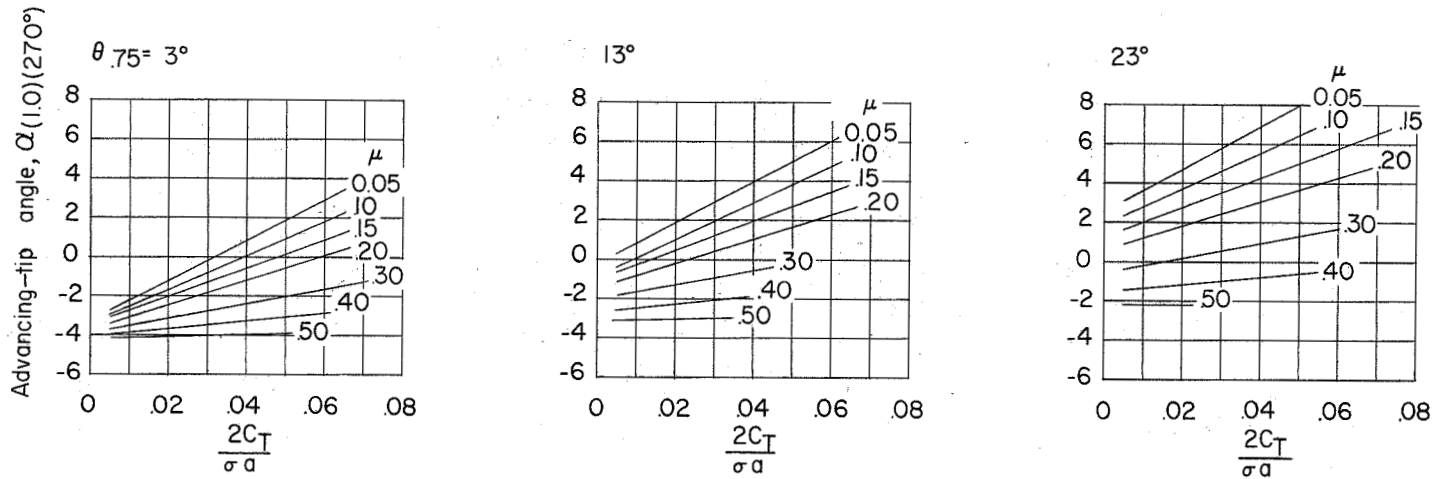
Figure 5.- Plots for estimating retreating-blade stall conditions.

(a) $\theta_1 = -8°$.

(b) $\theta_1 = -16°$.

Figure 6.- Plots for estimating advancing-tip angle of attack.